CLEAN TECHNOLOGY, Vol. 20, No. 2, June 2014, pp. 189~201

청정에너지기술

Synthesis Gas Production *via* Partial Oxidation, CO_2 Reforming, and Oxidative CO_2 Reforming of CH_4 over a Ni/Mg-Al Hydrotalcite-type Catalyst

Hoon Sub Song[#], Soon Jin Kwon[†], William S. Epling[‡], Eric Croiset*
Sung Chan Nam[§], and Kwang Bok Yi[#]*

Department of Chemical Engineering, University of Waterloo
200 University Ave. W., Waterloo, ON, N2L 3G1, Canada
[†]Graduate School of Energy Science and Technology, Chungnam National University
99 Daehak-ro, Yuseong-gu, Daejeon 305-764, Korea
[‡]Department of Chemical and Biomolecular Engineering, University of Houston
4800 Calhoun Road Houston, TX, 77004, United States
[§]Greenhouse Gas Department, Korea Institute of Energy Research
140, Yuseong-daero 1312beon-gil, Yuseong-gu, Daejeon 305-343, Korea
[#]Department of Chemical Engineering Education, Chungnam National University
99 Daehak-ro, Yuseong-gu, Daejeon 305-764, Korea

(Received for review March 26, 2014; Revision received May 14, 2014; Accepted May 16, 2014)

요 약

합성가스를 생산하기 위한 부분산화, 이산화탄소 리포밍, 메탄에 의한 산화CO_2 리포밍 공정들은 니켈 하이드로탈사이트($Ni_{0.5}Mg_{2.5}Al$) 촉매를 이용하여 수행되었고 안정한 이중층 구조를 형성시키기 위한 금속지지체(Mg, Ca)의 영향에 대해서도 다양한 연구가 진행되었다. 지지체전구물질(Mg, Ca)에 따라 메탄 리포밍의 안정성은 활성니켈이온과 지지체금속이온 사이의 결합강도차이에 의해 영향을 받는다. Ni-Mg-Al 구성체는 가장 안정한 하이드로탈사이트 이중층 구조이지만 Ni-Ca-Al 구성체는 그렇지 않다. 이산화탄소 리포밍 장기테스트에서 Ni-Mg-Al 촉매는 약 100시간 동안 80%의 효율을 유지하면서 탁월한 안정성을 보였지만 Ni-Ca-Al 촉매는 반응초기에 불활성화됨을 확인할 수 있었다. 활성금속 Ni과 지지체 Mg-Al 사이의 결합강도를 확인하기 위해 승온 환원(temperature-programmed reduction, TPR) 분석을 시행하였다. 이를 통해 Ni-Mg-Al 촉매가 Ni-Ca-Al 촉매보다 Ni의 환원온도가 더 높음을 확인할 수 있었다. $Ni_{0.5}Ca_{2.5}Al$ 촉매는 가장 높은 초기반응성을 보였지만 코크형성으로 인해 반응성이 빠르게 감소하였다. 결론적으로 $Ni_{0.5}Mg_{2.5}Al$ 촉매가 코크형성에 대한 강한 저항성을 갖고 있기 때문에 다른 촉매들보다 높은 반응성과 안정성을 갖는 것으로 보여진다.

주제어 : 메탄부분산화, 이산화탄소 리포밍, 산화개질, 하이드로탈사이트

Abstract : Partial oxidation, CO_2 reforming and the oxidative CO_2 reforming of CH_4 to produce synthesis gas over supported Ni hydrotalcite-type ($Ni_{0.5}Mg_{2.5}Al$ catalyst) catalysts were carried out and the effects of metal supports (i.e.; Mg and Ca) on the formation of a stable double-layer structure on the catalysts were evaluated. The CH_4 reforming stability was determined to be affected by the differences in the interaction strength between the active Ni ions and support metal ions. Only a Ni-Mg-Al composition produced a highly stable hydrotalcite-type double-layered structure; while the Ni-Ca-Al-type composition did not. Such structure provides excellent stability for the catalyst (-80% efficiency) as confirmed by the long-term CO_2 reforming test (-100 h), while the Ni-Ca-Al catalyst exhibited deactivation phases starting at the beginning of the reaction. The interaction strength between the active metal (Ni) and the supporting components (Mg and Al) was determined by temperature-programed reduction (TPR) analyses. The affinity was also confirmed by the TPR temperature because the Ni-Mg-Al catalyst required a higher temperature to reduce the Ni relative to the Ni-Ca-Al catalyst. The highest initial activity for synthesis gas production was observed for the $Ni_{0.5}Ca_{2.5}Al$ catalyst; however, this activity decreased quickly due to coke formation. The $Ni_{0.5}Mg_{2.5}Al$ catalyst exhibited a high reactivity and was more stable than the other catalysts because it had a higher resistance to coke formation.

Keywords : Methane partial oxidation, CO_2 reforming, Oxidative reforming, Hydrotalcite

1. Introduction

In recent years, the replacement of fossil fuels has received much attention as a result of various environmental issues as well as the limited amount of resources[1]. Therefore, the utili-

* To whom correspondence should be addressed.
E-mail: ecroiset@uwaterloo.ca, cosy32@cnu.ac.kr
doi: 10.7464/ksct.2014.20.2.189
pISSN 1598-9721 eISSN 2288-0690
http://cleantech.or.kr/ct/

zation of natural gas (mainly CH_4) for useful energy applications in transportation, such as methanol, hydrogen, or synthesis gas, is an attractive technology. There are many approaches to develop of highly resistant catalysts for the CH_4 reforming process and improve simultaneously the lifetime of the catalysts. One of the most common active metal components is Ni supported by stable materials (i.e.; Al_2O_3). Supported Ni catalysts are the typical choice for methane reforming, with Ni metal being an active component in CH_4 dissociation[2-4]. Typically, supported Ni catalysts are prepared by the wet-impregnation method. However, the catalysts prepared by wet-impregnation are often not fully capable of reduction by H_2 and the active Ni metal is often not homogenously distributed on/in the catalyst [5]. Additionally, Ni particles typically sinter during reformation reactions at high temperatures[6], and the larger Ni particle sizes promote carbon formation. Under reforming conditions, catalyst deactivation also leads to a reduction in pressure due to the build-up of carbonaceous species[4,7,8]. A catalyst with a homogeneously distributed active sites would therefore be more resistant to sintering and coke formation under extreme conditions[9-12]. Hydrotalcite (HT)-like compounds, a class of layered double hydroxides (LDHs), contain 2+ and 3+ metal ions randomly distributed throughout the layered structure. The Mg-Al HT precursors, based on $[Mg_{1-x}^{2+}Al_x^{3+}(OH)_2]^{x+}(CO_3^{-}{}_x)\cdot mH_2O$, in which a portion of the Mg^{2+} ions can be replaced by Ni^{2+}, contain exchangeable anions located within the layered structure[6,9,13,14]. Upon high temperature calcination, this type of catalyst maintains a high surface area. Additionally, the HT-type compounds contain very small crystallites comprising oxide mixtures, which are stable during high temperature reactions and can also be reduced to thermally stable metal particles[15, 16]. These attributes render the Mg-Al HT, with Ni substitution, an optimal catalyst candidate for reforming reactions. In recent years, many investigations have been conducted to increase the stability of the HT-type catalysts by adding promoters. For example, Yu inserted La into the Ni-Mg-Al HT catalyst to inhibit carbon formation and enhance CO_2 adsorption.

Eq. (1) represents the general expression of the combined partial oxidation reaction where CO_2 reforming is converted to CH_4, where x represents the amount of CO_2 added. The stoichiometric amount of oxygen can then be determined by the amount of CO_2 present. If x is zero, then Eq. (1) is equivalent to the partial oxidation reaction, Eq. (2). If x is 6, then Eq. (1) is equivalent to the CO_2 reforming reaction, Eq. (3). Changing x between 0 and 6 changes the H_2/CO ratio between 2 and 1. Therefore, by varying x, the resulting synthesis gas ratio (i.e. H_2/CO ratio) can be tailored to be between 2 and 1. For methanol production, the conversion of CO_2 reforming of methane would require an additional process to adjust the H_2/CO ratio because it results in a synthesis gas ratio less than 2[17,18]. The partial oxidation of CH_4, which meets the H_2/CO ratio of 2 for downstream methanol production, is difficult to control due to the formation of hot-spots and the subsequent risk of explosion[2]. In the oxidative CO_2 reforming of CH_4 (where x ranges from 0 to 6 in Eq. (1)), the H_2/CO ratio can be controlled by adjusting the feed ratio of O_2 and CO_2. Therefore, the oxidative CO_2 reforming of CH_4 is an interesting approach to synthesis gas production, especially for downstream applications with specific H_2/CO ratio needs, such as methanol synthesis or the Fischer-Tropsch process[19]. Additionally, the oxidative CO_2 reforming of CH_4 overcomes some of the limitations of independent partial oxidation and CO_2 reforming reactions[20]. For example, CO_2 reforming of CH_4 is endothermic and typically requires a substantial heat input to maintain the reaction temperatures. However, combining it with the partial oxidation reaction results in a lower energy input being required to maintain the catalyst bed at high temperatures, because the exothermic partial oxidation reaction can provide the heat for the endothermic reforming component[13].

$$6\ CH_4 + x\ CO_2 + (3\text{-}x/2)\ O_2 \leftrightarrow 12\ H_2 + (6+x)\ CO \quad (1)$$

$$CH_4 + 0.5\ O_2 \leftrightarrow 2\ H_2 + CO \quad (2)$$

$$CH_4 + CO_2 \leftrightarrow 2\ H_2 + 2CO \quad (3)$$

As described above, a variety of catalysts have been previously employed in steam reforming, partial oxidation, and dry reforming to produce synthesis gas. However, most of these studies did not include long-term experiments to determine the stability of the HT-type catalyst. In this study, a typical Ni-Mg/Al HT-type catalyst was used for synthesis gas production. Additionally, the effects of various cations on the formation of the HT-type catalyst were evaluated with respect to stability.

2. Experimental

2.1. Catalyst preparation

Two co-precipitated catalysts ($Ni_{0.5}Mg_{2.5}Al$ and $Ni_{0.5}Ca_{2.5}Al$) were prepared. The preparation procedure for both catalysts was identical, with either Mg or Ca nitrates being used as the precursors. For the preparation of the $Ni_{0.5}Mg_{2.5}Al$ catalyst, 30 mL of a 1 M Ni nitrate ($Ni(NO_3)_2\cdot 6H_2O$, Puratronic®, 99.9985%) aqueous solution, 150 mL of a 1 M Mg nitrate (magnesium nitrate hexahydrate, Alpha-Aesar, ACS grade 98.0-102.0%) aqueous solution and 60 mL of a 1 M Al nitrate ($Al(NO_3)_3\cdot 9H_2O$, Alpha-Aesar, ACS grade 98.0-102.0%) aqueous solution were prepared and mixed. The mixed nitrate solution was then

added drop-wise into 240 mL of a 0.50 M Na_2CO_3 aqueous solution at room temperature under vigorous stirring (400 rpm). A 3.0 M NaOH aqueous solution was simultaneously added drop-wise to maintain the pH at 10.0 ± 0.1. The resulting precipitate was aged in the mother liquor at 120 ℃ for 12 h. The aged precipitate was then cooled to room temperature and held for 1 h. The precipitate was then washed and filtered with distilled and de-ionized water until the residual Na^+ in the aged precipitate was removed (pH ~7). The washed precipitate was then dried at 120 ℃ for 12 h. The $Ni_{0.5}Ca_{2.5}Al$ catalyst was prepared in the same manner using a mixture of 30 mL of 1 M Ni nitrate, 150 mL of 1 M Ca nitrate ($Ca(NO_3)_2 \cdot 4H_2O$, Alpha-Aesar, ACS grade 98.0-102.0%), and 60 mL of 1 M Al nitrate. In preparing the 10 wt% Ni/Al_2O_3 catalyst, ~75 mL of distilled water was heated to 80 ℃ while stirring, and γ-Al_2O_3 powder (Alpha-Aesar, 99.97% (metal basis)) was then added to the distilled water. 1 M Ni nitrate was added drop-wise, until the target 10 wt% of Ni relative to the Al_2O_3 was obtained. For all catalysts, water was evaporated under continuous stirring at 80 ℃. The resulting residue was then heated in an oven at 120 ℃ for 12 h, and the dried precipitate was crushed to powder form. The powder precipitates were calcined at 850 ℃ in air for 5 h to produce an oxide-phase catalyst. The calcined catalysts were pelletized to attain a particle size of 354-500 μm.

2.2. Catalyst characterization

The catalyst crystal structures of the fresh and spent catalysts were characterized using X-ray diffraction (XRD). Powder XRD patterns were measured on a Rigaku D/Max-III C using standard Bragg-Brentano geometry with Ni-filtered Cu Kα radiation ($\lambda_1 = 1.5406$ Å, $\lambda_2 = 1.5444$ Å) and 40 kV/100 mA X-ray radiation. The XRD data were collected in the range of 5° to 80° 2θ range using a step size of 0.01 and a count time of 1 s. The diffraction patterns were identified upon comparison with spectra in the JCPDS data base (International Centre for Diffraction Data, USA). Catalyst surface areas were measured using a Micromeritics Gemini 3 2375. Approximately 100 mg of the pelletized catalysts (particle size in the range 354-500 μm) was loaded and the surface area was measured at -196 ℃, using liquid nitrogen as the adsorbate. Eleven points within the P/P_0 range of 0.05 and 0.3 were collected and used to produce the BET plot and subsequently calculate the surface area. The BET surface areas of the $Ni_{0.5}Mg_{2.5}Al$, $Ni_{0.5}Ca_{2.5}Al$, and Ni/Al_2O_3 catalysts after calcination and reduction are listed in Table 1 and compared to some reference values. After reduction in 10% H_2/N_2 at 720 ℃ for 1 h, the surface areas increased, which implied re-construction of the catalyst surfaces. The $Ni_{0.5}Ca_{2.5}Al$ catalyst had the highest increase in surface area after reduction.

The catalyst morphology was examined using scanning electron microscopy (SEM). A Leo FESEM 1530 SEM was utilized in this investigation, and the vacuum pressure was less than 1.5×10^{-5} mbar. TPR and TPO were also used to characterize the catalysts. For the TPR test, 100 mg of the calcined catalyst was placed in a quartz tube and the temperature was ramped at 10 ℃/min from 25 to 800 ℃ in the presence of a 10% H_2/N_2 reducing gas mixture flowing at 30 mL/min. A thermal conductivity detector (TCD) was then used to measure the amount of H_2 consumption. The amount of coke produced during the CO_2 reforming of CH_4 was determined by TPO in a Hiden Catlab micro-reactor system. 25 mg of the spent catalyst was placed in the quartz tube and a 30 mL/min 10% O_2/He gas mixture was utilized. The sample temperature was increased from 25 ℃ to 850 at 10 ℃/min.

Table 1. Catalyst surface areas after calcination and reduction

Catalysts	After calcination[a] (m^2/g)	After reduction[b] (m^2/g)	References
10 wt% Ni/Al_2O_3	191.0	191.2	This work
$Ni_{0.5}Ca_{2.5}Al$	33.2	55.7	
$Ni_{0.5}Mg_{2.5}Al$	149.0	153.0	
spc-Ni/Mg-Al	-	161.0	[18]
spc-Ni/Ca-Al	-	14.6	
imp-Ni/Al_2O_3	-	95.0	
$Ni_{0.5}/Mg_{2.5}(Al)O$	158.0	-	[17]
13.5 wt% Ni/γ-Al_2O_3	106.3	-	

[a]Calcined at 1,123 K for 5 h in air
[b]Reduced at 993 K for 1 h in 10% H_2/N_2

2.3. Catalytic reaction tests

A fixed-bed reactor was designed to examine the catalyst performances. The catalyst bed resided in a 10 mm I.D. quartz tube with a highly porous quartz frit to support the catalyst. A thermocouple located at the top of the catalyst bed was used to control the furnace temperature. Before the reaction tests, the effects of the external and internal mass transfer limitation at a constant GHSV of 240,000 cm^3/g-h were examined. For the external mass transfer, a fixed residence time ($W/F = 0.015$) through a variety of feed velocities (50, 100, 150, 200 and 250 mL/min of total feed) at 700 ℃ was chosen. The internal mass transfer was evaluated using a feed mixture composed of $CH_4/CO_2/N_2 = 1/1/3$ at 700 ℃ for various sizes of catalysts (average 303, 427, and 605 μm). When the CH_4 consumption rate was unchanged for the external and internal mass transfer limitations, the reaction can then be controlled by the reaction limitation instead of the diffusion limitation. The activation energy of CH_4 and CO_2 consumption was determined by the Arrhenius

plot. For each reaction test, 50 mg of the calcined catalyst with a particle size between 354-500 μm was diluted with 400 mg of SiC (422-599 μm). The SiC was used to prevent an increase in pressure due to coke formation and subsequently improve the thermal dispersion throughout the catalyst bed. The catalysts were reduced *in situ* at 720 ℃ in 200 mL/min of 10% H_2/N_2 for 1 h. After the reduction, the bed temperature was reduced to the desired reaction temperature under 100% N_2. During the catalyst activity tests, the total gas flow rate was set to 200 mL/min (80 mL/min of reactant gases and 120 mL/min of N_2). The feed ratio for the partial oxidation of CH_4 was $CH_4/O_2/N_2$ = 26/14/60 and for CO_2 reforming of CH_4 was $CH_4/CO_2/N_2$ = 20/20/60. For the oxidative CO_2 reforming of CH_4, the x represented the amount of CO_2 added in Eq. (1) was (4) in this study. The ratio was therefore $CH_4/CO_2/O_2/N_2$ = 21.8/14.5/3.6/60, and the stoichiometry corresponding to $x = 4$ is shown in Eq. (4).

$$6CH_4 + 4CO_2 + O_2 \leftrightarrow 12H_2 + 10CO \quad (4)$$

The resulting gases were collected and sampled using a gas chromatography (GC) column (Varian CP-3800 with a Carboxen-1000) to quantify the components of the product gases. The CH_4 conversion rate (Eq. (5)) and the synthesis gas ratio, H_2/CO, (Eq. (6)) were calculated from the concentrations measured by GC, which were then converted into molar flow rates. The activation energy of CH_4 and CO_2 were calculated from the Arrhenius plot (Eq. (7)).

$$-r'_{CH4}\left(\frac{mol}{g_{cat} * sec}\right) = \frac{dF_{CH4}}{dW} = \frac{X_i \times F_i(mol/min)}{W_{cat}(g)} \quad (5)$$

$$H_2/CO\ ratio = \frac{n_{H_2,out}}{n_{CO,out}} \quad (6)$$

For the pre-treatment, the catalysts were reduced at 720 ℃ in 10% H_2/N_2 for 1 h. The three reactions-partial oxidation, CO_2 reforming, and oxidative CO_2 reforming of CH_4-were carried out with a GHSV = 240,000 cm^3/g-h at 700 ℃ for 20 h during the first set of experiments.

3. Results and discussions

3.1. Catalyst activities

3.1.1. External and internal mass transfer limitation

Reliable kinetic data could be obtained when the mass transfer limitation (external and internal) was negligible. The effects of the feed flow rate and catalyst particle size on the reaction rate were experimentally determined using a feed mixture composed of $CH_4/CO_2/N_2$ (1/1/3) at 700 ℃. For the external diffusion, a constant rate (W/F = 0.015 g*s/mL) was applied in order to maintain the amount of contact time. The effects of the flow rate with a consistent amount of contact time are shown in Figure 1. It is clear that the rate of CH_4 consumption increased until the flow rate was 200 mL/min. This result indicated that up to the flow rate of 200 mL/min, the external mass transfer had some influence on the overall reaction rate. However, when the flow rate exceeded 200 mL/min, the rate of CH_4 consumption remained constant. Therefore, experiments with a flow rate of 200 mL/min are adequate to obtain reaction data that are not masked by the external transport limitation.

In order to investigate the possible effects of internal diffusion limitation, three different particle sizes were tested: (i) 251-354 μm (average 303 μm), (ii) 354-500 μm (average 427 μm), and (iii) 500-710 μm (average 605 μm). The flow rate was chosen to be 200 mL/min based on the external limitation. The

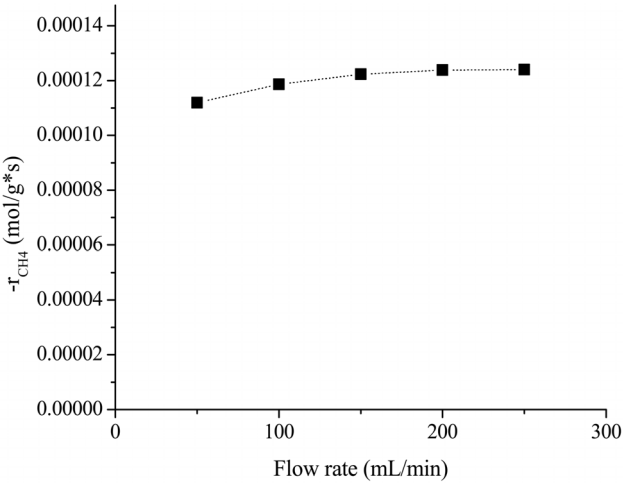

Figure 1. External mass transfer limitation (Catalyst: $Ni_{0.5}Mg_{2.5}Al$-HT; W/F = 0.015 at 700 ℃).

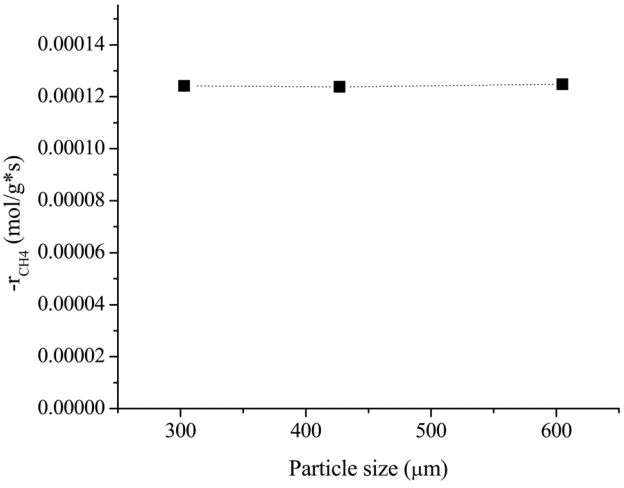

Figure 2. Internal mass transfer limitation (Catalyst: $Ni_{0.5}Mg_{2.5}Al$-HT; Feed flow rate = 200 mL/min at 700 ℃).

effects of the particle size on the rate of CH_4 consumption is shown in Figure 2. It was clear that the rate of CH_4 consumption was independent of the average diameter of the particles. This result indicated that particle sizes between 250 and 700 μm are small enough for the reaction to not be affected by internal mass limitation at 700 ℃.

3.1.2. Partial oxidation of CH_4

The conversions attained during the CH_4 partial oxidation and the resulting synthesis gas ratios (H_2/CO) are shown in Figure 3. All catalysts exhibited -85% CH_4 conversion and the Mg- and Ca-containing samples exhibited no significant deactivation over the 20 h test. Additionally, the levels of reactivity were all determined to be near the equilibrium levels. The Ni/Al_2O_3 catalyst exhibited some deactivation beginning after 13 h of reaction, which confirmed that the Ni/Al_2O_3 catalyst deactivates over time, as confirmed by many other previous studies[21-23]. The synthesis gas ratios (H_2/CO ratio) obtained with each catalyst exhibited similar patterns. The $Ni_{0.5}Mg_{2.5}Al$ and $Ni_{0.5}Ca_{2.5}Al$ catalysts resulted in a syngas ratio of around 2, close to the theoretical level. This result indicated that since H_2 and CO were produced in proportion, the stoichiometry in Eq. (4) was applied and neither product was preferentially consumed via side reactions afterwards. The syngas ratio decreased with time over the Ni/Al_2O_3 catalyst, which corresponded to the reduced conversion. In conclusion, for the partial oxidation of CH_4, the two co-precipitated catalysts ($Ni_{0.5}Mg_{2.5}Al$ and $Ni_{0.5}Ca_{2.5}Al$) exhibited stable reactivity for 20 h of reaction with conversions close to the equilibrium level and syngas ratios near the predicted values based on the reaction stoichiometry.

3.1.3. CO_2 reforming of CH_4

Coke covering the active Ni sites will ultimately lower the activity of the catalyst. It is therefore assumed that the dry reforming is a good indicator of the carbon deposition resistance of a given catalyst. Under CO_2 reforming of CH_4, two reactions typically occur CO_2 reforming of CH_4 (Eq. (3)) and the reversible water-gas shift (RWGS) reaction (Eq. (7)). Therefore, in addition to the main reaction, the RWGS also affects the overall pathway. For example, due to the RWGS reaction, the syngas ratio (H_2/CO) for CO_2 reforming of CH_4 was always less than 1.

$$CO_2 + H_2 \leftrightarrow CO + H_2O \quad (7)$$

The CH_4 conversions at 700 ℃ for the three catalysts, along with the equilibrium conversion, are shown in Figure 4. At 700 ℃, the theoretical CH_4 conversion level was -82%. The CH_4 conversion using the $Ni_{0.5}Ca_{2.5}Al$ catalyst increased slightly at the beginning and reached the equilibrium CH_4 conversion (82%) within 4 h time-on-stream. However, after 4 h it slowly deactivated over time, decreasing from 82% to 75% after 20 h. This reduction was likely caused by carbon build-up on the surface, which was confirmed by TPO and will be discussed later. The Ni/Al_2O_3 catalyst exhibited continuous deactivation from an initial CH_4 conversion of 60%, decreasing to 48% conversion after 20 h. It is important to note that Ni/Al_2O_3 also had the lowest initial CH_4 conversion. Alternatively, the $Ni_{0.5}Mg_{2.5}Al$ catalyst exhibited very stable conversion (-68%) compared to the other catalysts. This result indicates that the $Ni_{0.5}Mg_{2.5}Al$ catalyst exhibited the highest resistance to deactivation. However, the conversion was lower than the equilibrium conversion, and lower than the conver-

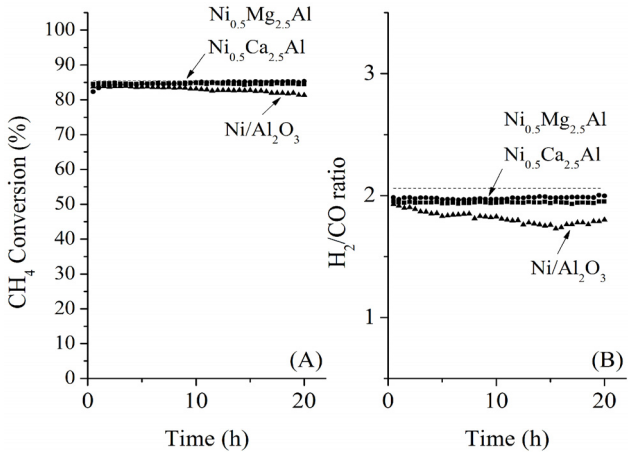

Figure 3. CH_4 conversion profiles and gas ratios (H_2/CO) for the CH_4 partial oxidation as a function of time for the three catalysts. Equilibrium values, calculated using ASPEN Plus™, are also plotted (total gas flow rate: 200 mL/min; $CH_4/O_2/N_2$ = 26/14/60 vol%; GHSV = 240,000 cm^3/g_{cat}-h).

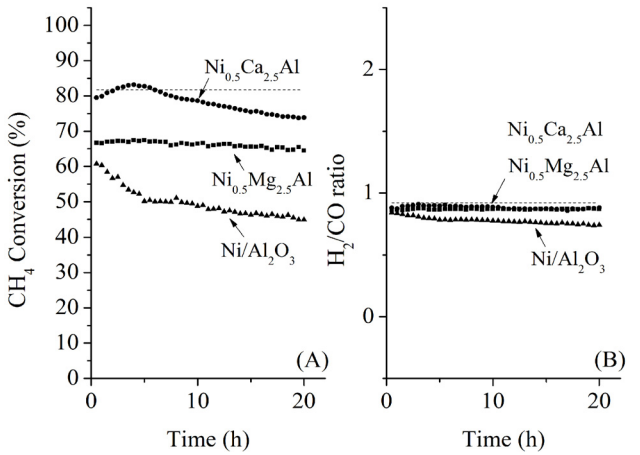

Figure 4. CH_4 conversion profiles and synthesis gas ratios (H_2/CO) as a function of time for CO_2 reforming of CH_4 using the three different catalysts (total gas flow rate: 200 mL/min; $CH_4/CO_2/N_2$ = 20/20/60 vol%; GHSV = 240,000 cm^3/g_{cat}-h).

sion obtained with the Ca-containing catalyst. The syngas ratios (H_2/CO ratios) were also less than unity due to the reverse water-gas shift (RWGS) reaction (Eq. (7)). Additionally, even though the CH_4 conversion over the three catalysts was distinguishable, the syngas ratios were very similar and all catalysts started with a ratio of -0.9, which was close to the equilibrium value. These results confirmed that the CH_4 conversions were dependent on the catalysts, but the synthesis gas ratios were not, which suggested that the same reaction pathway was occurring over each catalyst. These results also indicated that the RWGS reaction rapidly reaches equilibrium for CO_2 reforming of CH_4 at 700 ℃.

During 20 h of time-on-stream, the $Ni_{0.5}Mg_{2.5}Al$ catalyst exhibited high stability, and the $Ni_{0.5}Ca_{2.5}Al$ catalyst exhibited deactivation. However, even after 20 h, the activity of the Ca-based catalyst was still higher than the Mg-based catalyst. It is therefore difficult to conclude after 20 h time-on-stream which of these two catalysts was better. Therefore, more prolonged experiments were performed at 100 h time-on-stream for these two catalysts. The pre-treatment processes were identical to those described previously. The experimental results for the $Ni_{0.5}Mg_{2.5}Al$ catalyst and the $Ni_{0.5}Ca_{2.5}Al$ catalyst are shown in Figure 5 for over 100 h of the dry reforming. The $Ni_{0.5}Mg_{2.5}Al$ catalyst exhibited a relatively stable reactivity based on the CH_4 conversion and the H_2/CO ratio. The CH_4 conversion decreased by about 4% over 100 h, from 67 to 63%. However, for the $Ni_{0.5}Ca_{2.5}Al$ catalyst, the deactivation trend observed during the first 20 h continued throughout 100 h. The CH_4 conversion decreased from 78 to 62% but the syngas ratio only slightly decreased. Based on these longer-term experiments, it was clear that the $Ni_{0.5}Mg_{2.5}Al$ catalyst suffered considerably less deactivation than the $Ni_{0.5}Ca_{2.5}Al$ catalyst and exhibited a much higher resistance to coke formation, as will be discussed below. In conclusion, the $Ni_{0.5}Mg_{2.5}Al$ catalyst exhibited the highest stability, even though the activity remained lower than the equilibrium-based expectation. The $Ni_{0.5}Ca_{2.5}Al$ catalyst initially exhibited the highest activity, reaching equilibrium after about 4 h time-on-stream, but past 4 h its activity continuously decreased at a rate of -0.2%/h. Finally, the Ni/Al_2O_3 catalyst exhibited the worst reactivity and stability for the dry reforming.

3.1.4. Oxidative CO_2 reforming of CH_4

The basic concept of the oxidative CO_2 reforming of CH_4 is to combine the exothermic partial oxidation with the endothermic CO_2 reforming. The change in reaction enthalpy (ΔH) at 700 ℃ for the range of x [Eq. (1)] between 0 and 6 was simulated using ASPEN Plus™, the results of which are shown in Figure 6. When x was 0, Eq. (1) represented the partial oxidation of the CH_4 reaction and when x was 6, it represented the CO_2 reforming of CH_4. Figure 6 confirms that oxidative CO_2 reforming of CH_4 at 700 ℃ was an endothermic reaction when x was greater than 1. In order to confirm the ASPEN simulation (Figure 6) with actual experimental data, temperature data obtained during the experiments are shown in Figure 7. With the two reforming reactions, there was an immediate decrease in temperature, which then increased as the heat of the furnace compensated for the drop in temperature. For the partial oxidation reaction, the opposite process occurred. The oxidative reforming led to a smaller decrease in temperature relative to the dry reforming alone, confirming that the former requires less heat to maintain the reaction temperature while reducing the chance of hot spots formation as a result of partial oxidation.

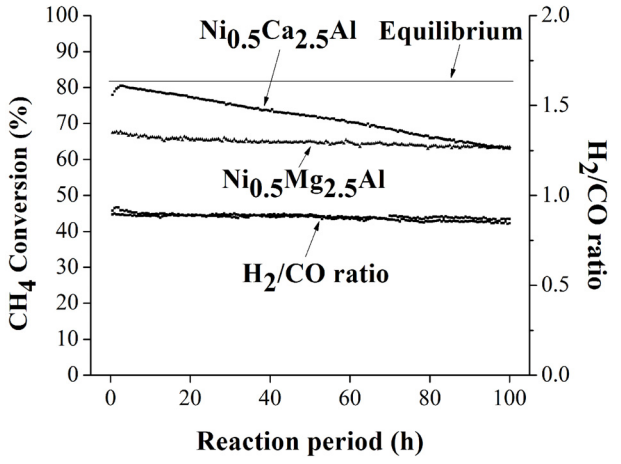

Figure 5. Long-term $Ni_{0.5}Mg_{2.5}Al$ and $Ni_{0.5}Ca_{2.5}Al$ catalytic performance profiles for CO_2 reforming of CH_4 (total gas flow rate: 200 mL/min; $CH_4/CO_2/N_2$ = 20/20/60 vol%; GHSV = 240,000 cm^3/g_{cat}-h).

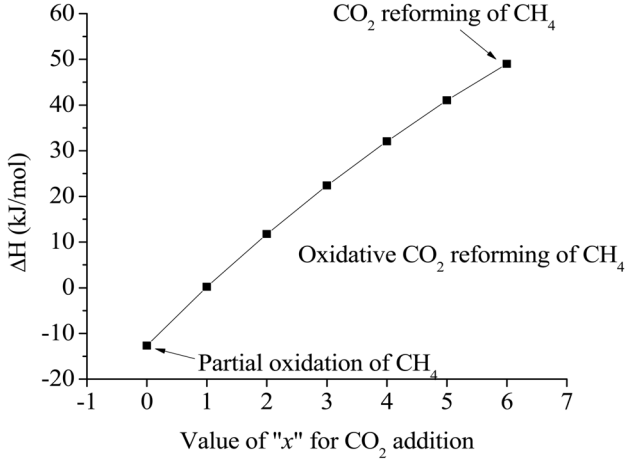

Figure 6. Change in enthalpy (ΔH) at 700 ℃ as a function of the x value described in Eq. (1) (calculated using ASPEN Plus™).

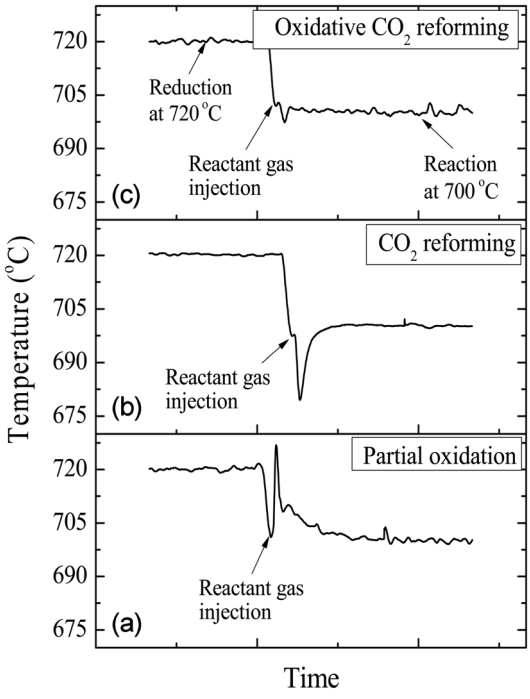

Figure 7. Temperature profiles during partial oxidation, CO_2 reforming, and the oxidative CO_2 reforming of CH_4 upon reducing the reaction temperature from 720 ℃ to 700 ℃.

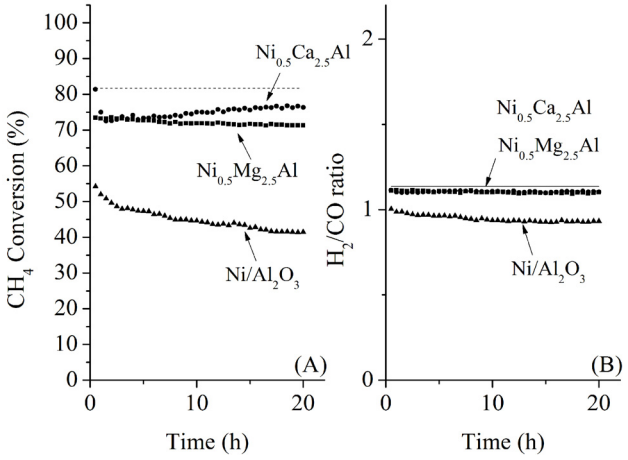

Figure 8. CH_4 conversion profiles and synthesis gas ratios (H_2/CO) for the oxidative CO_2 reforming of CH_4 on the three catalysts (total gas flow rate: 200 mL/min; $CH_4/CO_2/O_2/N_2$ = 21.8/14.5/3.6/60 vol%; GHSV = 240,000 cm^3/g_{cat}-h).

The catalytic activities for the oxidative CO_2 reforming of CH_4 over the three catalysts are shown in Figure 8. Co-feeding O_2 with CH_4 and CO_2 was expected to reduce carbon deposition as a result of the increased oxidation of surface carbon species and also increase the conversion of CH_4 at high temperatures (-700 ℃). The reactivities of the $Ni_{0.5}Ca_{2.5}Al$ and $Ni_{0.5}Mg_{2.5}Al$ catalysts during the initial period (< 5 h) were similar (-75%). The reactivity of the $Ni_{0.5}Ca_{2.5}Al$ catalyst for oxidative CO_2 reforming of CH_4 was less than that of CO_2 reforming of CH_4; however, the reactivity of the $Ni_{0.5}Mg_{2.5}Al$ catalyst was quite similar. Since the feed for the oxidative CO_2 reforming of CH_4 contains oxygen that might oxidize surface carbon, the $Ni_{0.5}Ca_{2.5}Al$ catalyst did not exhibit deactivation, and conversion actually slightly increased after 20 h of reaction. The syngas ratios for the catalysts were similar, even though the syngas ratio for the Ni/Al_2O_3 was slightly lower than that of the other catalysts. These trends (different conversions but same syngas ratios) were also observed in the partial oxidation and CO_2 reforming reactions, which suggested that the same reaction mechanisms existed over the three sample types. Additionally, except for the Ni/Al_2O_3 catalyst, the H_2/CO ratio was very close to its equilibrium value, which implied that the RWGS reaction reached equilibrium in the presence of the $Ni_{0.5}Mg_{2.5}Al$ and $Ni_{0.5}Ca_{2.5}Al$ catalysts at 700 ℃.

Overall, based on the reactivity tests for all three sets of reactions, the $Ni_{0.5}Mg_{2.5}Al$ catalyst exhibited the most stable reactivity among other catalysts under the most severe conditions (e.g. CO_2 reforming of CH_4). Additionally, the reactivity of the $Ni_{0.5}Mg_{2.5}Al$ catalyst, although lower than the equilibrium conversion, still resulted in greater than 70% CH_4 conversion. The $Ni_{0.5}Ca_{2.5}Al$ catalyst exhibited the highest initial CH_4 conversion for all reactions; however, its reactivity began to degrade shortly after the onset of the dry reforming test. Finally, as expected, the tests on oxidative CO_2 reforming of CH_4 exhibited convertsions between those of the partial oxidation and the dry reforming. An important difference between the oxidative CO_2 reforming and dry reforming in the presence of the $Ni_{0.5}Ca_{2.5}Al$ catalyst was that the reactivity was more active when oxygen was added and its activity decreased initially but eventually stabilized at a level similar to that of $Ni_{0.5}Mg_{2.5}Al$. Nonetheless, the $Ni_{0.5}Mg_{2.5}Al$ catalyst exhibited superior stability under dry reforming and oxidative reforming.

3.1.5. Activation Energy and Effects of the Partial Pressures of CH_4, CO_2, and H_2

Typically, the kinetic studies were conducted at the temperature in which the conversion was far from the equilibrium. It was confirmed that the CH_4 consumption rate from the reactivity test (Figure 4) at 700 ℃ was lower than the equilibrium level. The temperature sensitivity of the CH_4 consumption rate for CO_2 reforming of CH_4 over the $Ni_{0.5}Mg_{2.5}Al$-HT catalyst was determined by the Arrhenius plot (Figure 9) in the temperature range of 650-750 ℃ at a constant GHSV of 240,000 cm^3/g-h. It was clear that the support of Ni crystallites significantly influenced the activation energy by affecting the rate-controlling step in the reaction sequence. The activation energy for the consumption of CH_4 and CO_2 and the formation of H_2 and CO on the $Ni_{0.5}Mg_{2.5}Al$-HT catalyst were calculated to be 18.9, 18.0,

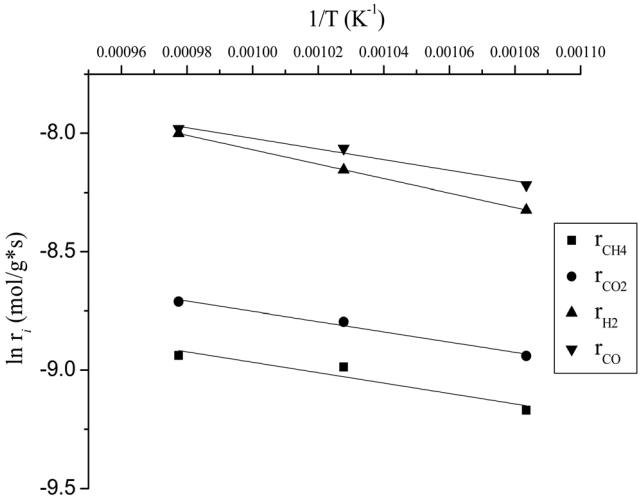

Figure 9. Arrhenius plot for CH_4 and CO_2 consumption at GHSV = 240,000 cm^3/g*h; Feed composition: $CH_4/CO_2/N_2$ = 1/1/3 vol%).

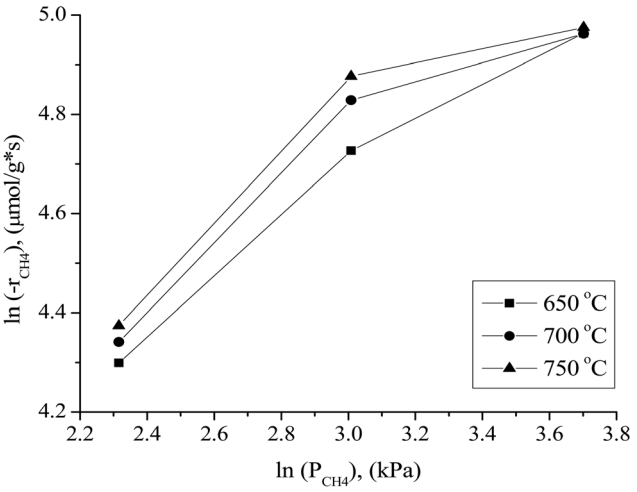

Figure 10. CH_4 consumption rate as a function of P_{CH_4} at a constant P_{CO_2} of 20.26 kPa.

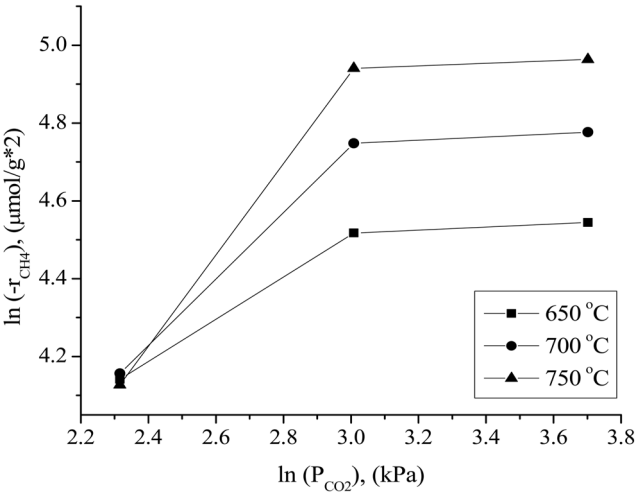

Figure 11. CH_4 consumption rate as a function of P_{CO_2} at a constant P_{CH_4} of 20.26 kPa.

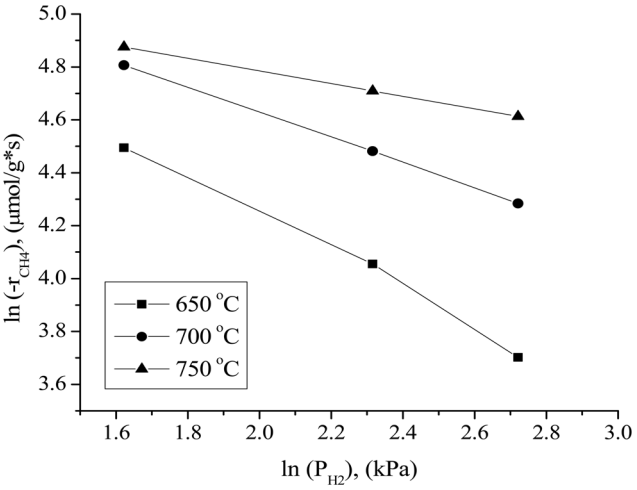

Figure 12. CH_4 consumption rate as a function of P_{H_2} at a constant P_{CH_4} and P_{CO_2} of 20.26 kPa.

25.3, and 18.7 kJ/mol, respectively. Based on the present investigation, it was determined that the rate determining step of CO formation closely corresponds to the CH_4 and CO_2 consumption step. One possible reason for obtaining a high energy barrier for H_2 formation was the RWGS process. Since the activation energy barrier of the CH_4 consumption step was slightly greater than that of the CO_2 consumption step, it was assumed that the CH_4 dissociation step could be the rate determining step. The lower activation energy barrier for CO_2 consumption might be caused by the presence of the strong Lewis base MgO, which can facilitate the activation of CO_2.

The influence of the partial pressures of CH_4, CO_2, and H_2 on the $Ni_{0.5}Mg_{2.5}Al$-HT catalyst at atmospheric pressure for the CH_4 consumption rate ($-r_{CH4}$) was evaluated in the temperature range of 650-750 ℃. A constant CO_2 (or CH_4) partial pressure of 20.26 kPa was used as the CH_4 (or CO_2) partial pressure was varied. N_2 gas was used to balance the total GHSV to 240,000 cm^3/g-h for all conditions. As shown in Figure 10, the CH_4 consumption rate was strongly affected by the partial pressure of CH_4 at a CO_2 partial pressure of 20.26 kPa, since the CH_4 consumption rate increased as the CH_4 partial pressure increased. As shown in Figure 11, the CH_4 consumption rate was strongly influenced when the partial pressure of CO_2 was lower (in the range of 10.13 to 20.26 kPa) than the stoichiometric ratio. The CH_4 consumption rate was then unchanged at higher CO_2 partial pressures (>20.26 kPa). Therefore, it can be concluded that the reaction rate was more sensitive to the CO_2 partial pressure than to the CH_4 partial pressure when compared in the low partial pressure ranges (10.13 to 20.267 kPa). However, at high CO_2 and CH_4 partial pressures (>20.26 kPa), the CH_4 partial pressure exhibited a stronger influence on the CH_4 consumption rates than

the CO_2 partial pressure. These results can be attributed to the stronger adsorption of CH_4 to the surface of the catalyst compared to that of CO_2 at higher partial pressures. Figure 12 displays the rates of CH_4 consumption at various partial pressures of H_2 at constant CH_4 and CO_2 partial pressures of 10.13 kPa. As the H_2 partial pressure increased, the rate of CH_4 consumption decreased because the reverse reaction and RWGS reaction then become dominant.

3.2. Catalyst characterization

3.2.1. Structure of fresh and spent catalysts

The fresh $Ni_{0.5}Mg_{2.5}Al$ and $Ni_{0.5}Ca_{2.5}Al$ catalyst crystal structures were investigated using XRD, and all diffraction patterns were matched with JPCDS references. The XRD patterns obtained from the $Ni_{0.5}Mg_{2.5}Al$ sample (Figure 13) confirmed that the as-prepared samples contained a well-crystallized HT-type (or LDH) phase. The LDH structure for the $Ni_{0.5}Mg_{2.5}Al$ catalyst implied that Ni^{2+} was incorporated in the Mg^{2+} site positions and dispersed uniformly throughout the brucite layer of the HT structure. In particular, a set of three reflection peaks at 2θ values of 11.3, 22.7, and 34.5° indicated that the HT-type structure possessed a layered structure in which both Ni^{2+} and Al^{3+} substituted Mg^{2+} sites in the brucite-like sheet[15,24]. After calcination at 820 ℃ in air for 5 h, the HT peaks disappeared and MgO (at 37.0, 43.1, 62.6, and 79.0°) and NiO (at 37.0, 43.1, 62.6, 74.9, and 79.0°) peaks appeared and overlapped. After reduction at 720 ℃ in 10% H_2/N_2 for 1 h, the NiO peaks were weak and the Ni metal peaks at 44.1, 51.7, and 76.1° were clearly visible. This result indicated that during reduction, some of the NiO crystals transformed into active Ni metal phases, as expected. Therefore, the $Ni_{0.5}Mg_{2.5}Al$ catalyst prepared by the co-precipitation method clearly contained active Ni phases substituted into a portion of the Mg^{2+} phases, resulting in the Ni/Mg-Al HT-type catalyst[25]. After thermal treatment at 850 ℃ in air for 5 h, and the reduction by 10% diluted H_2/N_2 at 720 ℃ for 1 h, the active Ni phases within the LDH become the active catalytic metal.

For the $Ni_{0.5}Ca_{2.5}Al$ catalyst, the XRD patterns of the fresh, calcined, and reduced catalysts are shown in Figure 14. The fresh $Ni_{0.5}Ca_{2.5}Al$ catalyst did not exhibit the HT-like structure. However, after being calcined at 820 ℃ in air for 5 h, NiO, CaO, and $Ca_{12}Al_{14}O_{33}$ peaks appeared. Interestingly, Ni metal peaks were observed with the calcined $Ni_{0.5}Ca_{2.5}Al$ catalyst but not with the $Ni_{0.5}Mg_{2.5}Al$ catalyst, which implied that the Ni-Ca interaction was weaker than Ni-Mg interaction.

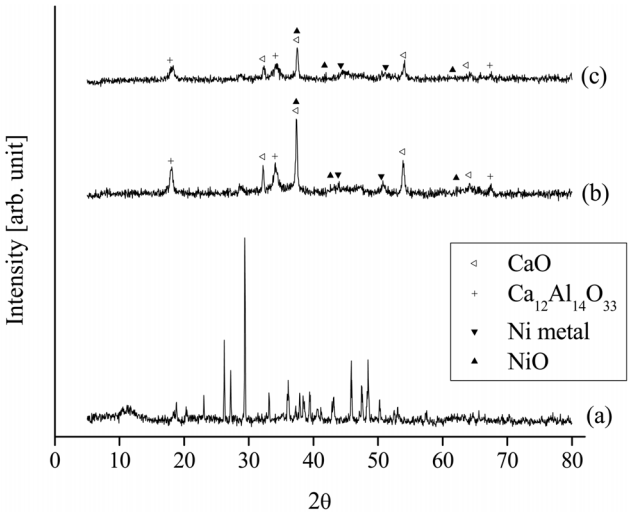

Figure 14. XRD patterns obtained from the $Ni_{0.5}Ca_{2.5}Al$ catalyst: (a) fresh; (b) calcined at 820 ℃ in air for 5 h; (c) reduced at 720 ℃ in 10% H_2/N_2 for 1 h.

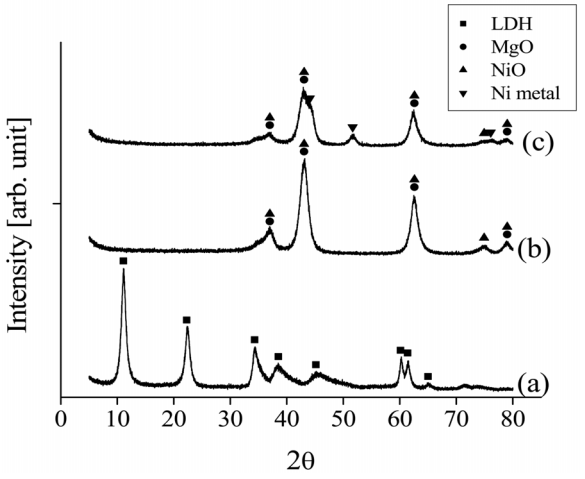

Figure 13. XRD patterns obtained from the $Ni_{0.5}Mg_{2.5}Al$ catalyst: (a) fresh; (b) calcined at 820 ℃ in air for 5 h; (c) reduced at 720 ℃ in 10% H_2/N_2 for 1 h.

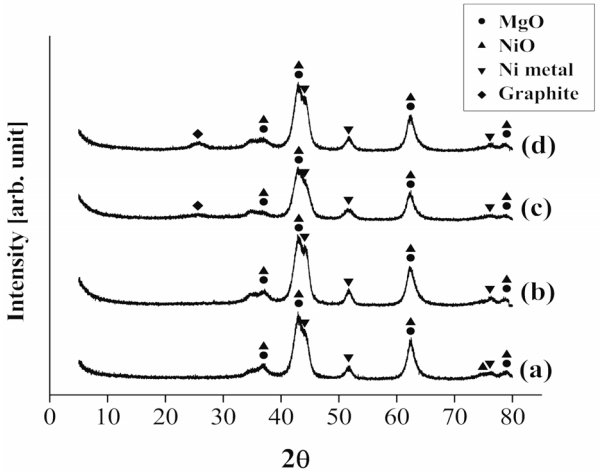

Figure 15. XRD patterns obtained from the $Ni_{0.5}Mg_{2.5}Al$ catalyst (a) after reduction; (b) after partial oxidation of CH_4; (c) after CO_2 reforming of CH_4; (d) after the oxidative CO_2 reforming of CH_4.

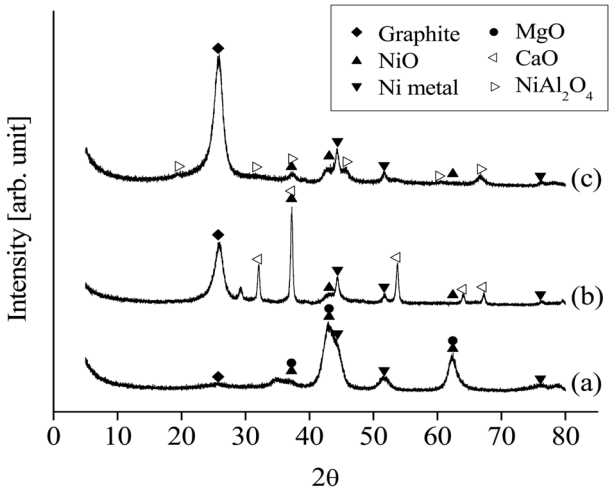

Figure 16. XRD patterns after CO_2 reforming of CH_4 at 700 ℃ for 20 h from: (a) $Ni_{0.5}Mg_{2.5}Al$; (b) $Ni_{0.5}Ca_{2.5}Al$; (c) Ni/Al_2O_3 catalysts.

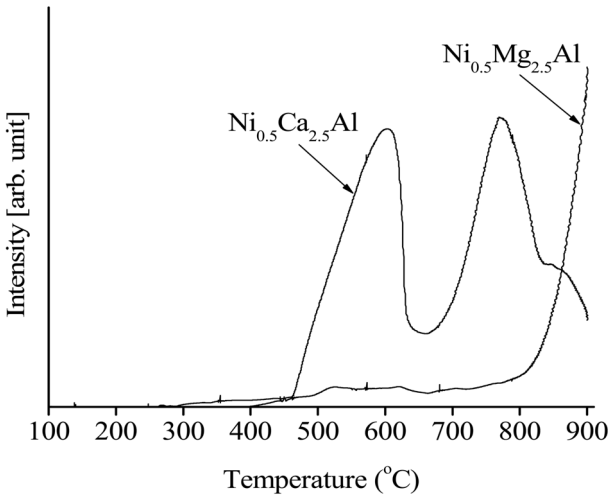

Figure 17. TPR results for the calcined $Ni_{0.5}Ca_{2.5}Al$ and $Ni_{0.5}Mg_{2.5}Al$ catalysts.

The XRD patterns of the spent $Ni_{0.5}Mg_{2.6}Al$ catalysts after 20 h of partial oxidation, CO_2 reforming and the oxidative CO_2 reforming of CH_4 at 700 ℃ are shown in Figure 15. Both Ni metal and NiO phases were observed after CH_4 partial oxidation and the oxidative CO_2 reforming of CH_4. The oxygen species supplied for the partial oxidation of CH_4 and the oxidative CO_2 reforming of CH_4 likely oxidized some of the Ni. However, the H_2 or CO generated from the reactions can simultaneously reduce the formed NiO, subsequently regenerating the active Ni phases for further reactions, resulting in evidence of both chemical states being present. Additionally, a weak graphite peak was observed at 26.4° after CO_2 reforming of CH_4 and the oxidative CO_2 reforming of CH_4 tests, but not after the CH_4 partial oxidation. The likely reason for its absence during partial oxidation is that the C:O ratio was the lowest (26:28) compared to the other two processes.

The XRD patterns of the different catalysts after 20 h of CO_2 reforming of CH_4 at 700 ℃ are shown in Figure 16. The diffraction patterns of $Ni_{0.5}Mg_{2.5}Al$ indicated the presence of both metal and oxide Ni, as well as MgO. However, the XRD data obtained from the $Ni_{0.5}Ca_{2.5}Al$ exhibited weaker Ni peaks, with significantly less Ni metal being observed. Most importantly, much stronger graphite peaks were observed on the $Ni_{0.5}Ca_{2.5}Al$ and Ni/Al_2O_3 catalysts than on the $Ni_{0.5}Mg_{2.5}Al$ catalyst. These results implied that the $Ni_{0.5}Mg_{2.5}Al$ catalyst had a stronger resistance to coke formation.

3.2.2. TPR of catalysts

The H_2-temperature-programmed reduction (H_2-TPR) data obtained from the calcined $Ni_{0.5}Mg_{2.5}Al$ and $Ni_{0.5}Ca_{2.5}Al$ catalysts are shown in Figure 17. The reducibility of the Ni-based catalysts during the reduction process was an important factor in determining the level of reactivity since metallic Ni produced by the reduction process was in the active phase to initiate the reaction (e.g. CH_4 dissociation). The reducibility of the catalyst was affected by, and can be estimated by measuring, the strength of the interaction between the active phase and the support. The $Ni_{0.5}Mg_{2.5}Al$ catalyst exhibited a small peak at low temperatures (~600 ℃) and slightly increased at high temperatures (<700 ℃) while the $Ni_{0.5}Ca_{2.5}Al$ catalyst exhibited two reduction peaks at lower temperatures, 580 and 770 ℃. Those two peaks can be assigned to complex NiO_x species corresponding to Ni/support interactions[39]. Since the $Ni_{0.5}Mg_{2.5}Al$ catalyst did not exhibit any H_2 consumption until very high temperatures were reached (>750 ℃), it was determined that the $Ni_{0.5}Ca_{2.5}Al$ catalyst exhibited relatively free NiO species. Previous investigations confirmed that the reduction process for the NiO-MgO would be initiated at very high temperatures (~900 ℃) since it produced a solid solution[26]. Additionally, the area under the TPR curve was clearly greater for $Ni_{0.5}Ca_{2.5}Al$ than for $Ni_{0.5}Mg_{2.5}Al$ and it can therefore be concluded that more Ni was reduced over the $Ni_{0.5}Ca_{2.5}Al$ catalyst compared to the $Ni_{0.5}Mg_{2.5}Al$ catalyst. This result also implied that the $Ni_{0.5}Mg_{2.5}Al$ catalyst exhibited stronger interactions between the Ni and support since the reduction peaked at a higher temperature over the $Ni_{0.5}Mg_{2.5}Al$ catalyst. These phenomena could be explained by comparing of the MgO, CaO, and NiO lattice sizes. Both MgO and CaO are face-centered cubic type oxides. However, only MgO has lattice parameters (a = 4.2112 Å) and bond distances (A-B = 2.11 Å) close to those of NiO (a = 4.1946 Å, A-B = 2.10 Å), with the lattice parameters and bond distances of CaO being a = 4.8105 Å and A-B = 2.40 Å[27]. This result suggested that NiO can be more easily substituted into the MgO lattice[24,28]. A catalyst that is more sus-

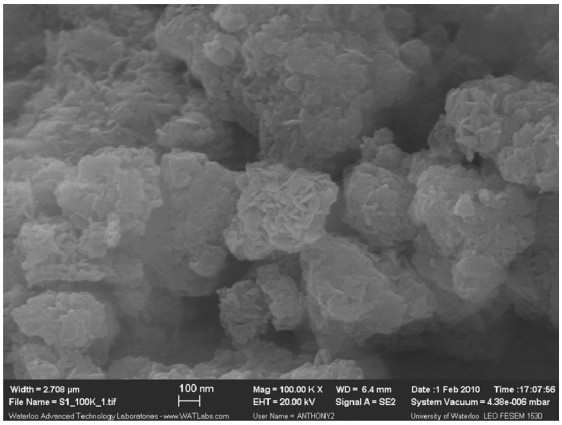

Figure 18. SEM of the fresh $Ni_{0.5}Mg_{2.5}Al$ catalyst (100,000× magnification).

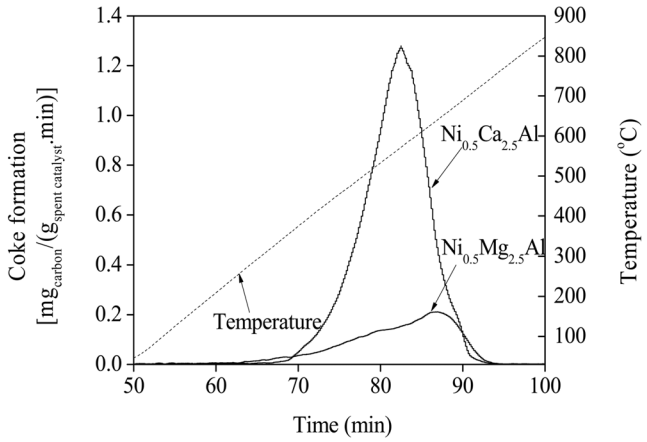

Figure 19. TPO results for $Ni_{0.5}Ca_{2.5}Al$ and $Ni_{0.5}Mg_{2.5}Al$ catalysts after CO_2 reforming of CH_4 at 700 ℃ for 20 h.

ceptible to reduction can ultimately provide more active sites on the catalytic surface, leading to higher reactivity. Based on the TPR results, the $Ni_{0.5}Ca_{2.5}Al$ was the more reducible catalyst and had higher initial reactivity in the partial oxidation, CO_2 reforming and the oxidative CO_2 reforming of CH_4 processes relative to the $Ni_{0.5}Mg_{2.5}Al$ catalyst, as shown in the reactivity data (Figure 3, Figure 4, and Figure 8). Additionally, since 720 ℃ was the reduction temperature used prior to the catalytic testing, the $Ni_{0.5}Mg_{2.5}Al$ catalyst was only partially reduced.

SEM images of the fresh $Ni_{0.5}Mg_{2.5}Al$ catalyst are shown in Figure 18, which display a layered structure (also referred to as a "card house" shape[15]) at the surface of the catalyst. Alternatively, the $Ni_{0.5}Ca_{2.5}Al$ catalyst did not exhibit a layered structure [27]. This result corresponds with the XRD results (Figure 13), where the data indicated that the $Ni_{0.5}Mg_{2.5}Al$ catalyst possessed a layered structure. Additionally, this layered structure provided stronger interactions between the active site (Ni) and the support (Mg-Al), resulting is a lower reducibility, as confirmed above.

3.2.3. Carbon deposition analysis

TPO experiments were performed to estimate the amount of carbon deposited on the catalytic surface after the reaction. The temperature of the catalyst bed was increased from 25 to 850 ℃ at a rate of 10 ℃/min. Mass spectrometry (MS) was used to detect the carbon oxides formed, which was then used to determine the amount of carbon present. The amount of carbon deposited on the catalysts can be estimated by calculating the area under the TPO curves plotted in Figure 19. The amounts of carbon deposited are listed in Table 2 and confirm that the $Ni_{0.5}Mg_{2.5}Al$ catalyst exhibited a significantly stronger resistance to coke formation relative to the $Ni_{0.5}Ca_{2.5}Al$ catalyst. The resistance to coke formation might be related to the stronger interaction between Mg and Ni ions, which subsequently inhibited coke formation. Alternatively, the $Ni_{0.5}Ca_{2.5}Al$ catalyst, which

Table 2. Amount of carbon deposition on the $Ni_{0.5}Mg_{2.5}Al$ and $Ni_{0.5}Ca_{2.5}Al$ catalysts after 20 h, CO_2 reforming at 700 ℃.

Catalysts	Coke (wt%)	Reference
$Ni_{0.5}Mg_{2.5}Al$	2.9	This work
$Ni_{0.5}Ca_{2.5}Al$	11.9	
spc-Ni/Mg-Al	Trace	[18]
spc-Ni/Ca-Al	0.2	
Ni/MgO	5.2	[22]

was more easily reduced and resulted in Ni/Ca interactions being weaker, was more susceptible to deactivation via coke build-up.

SEM images of spent $Ni_{0.5}Mg_{2.5}Al$ (Figure 20) and spent $Ni_{0.5}Ca_{2.5}Al$ (Figure 21) catalysts after 20 h of CO_2 reforming of CH_4 at 700 ℃ exhibited significant differences in the carbon deposition traits. Using the $Ni_{0.5}Mg_{2.5}Al$ catalyst resulted in significantly less carbon fiber evidence relative to the $Ni_{0.5}Ca_{2.5}Al$ catalyst.

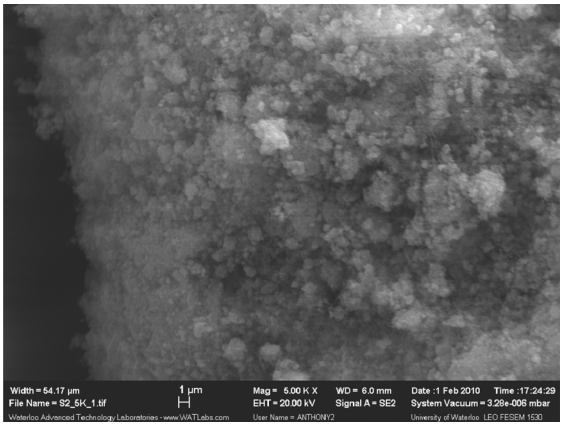

Figure 20. Spent $Ni_{0.5}Mg_{2.5}Al$ catalyst after 20 h of CO_2 reforming of CH_4 (5,000 × magnification).

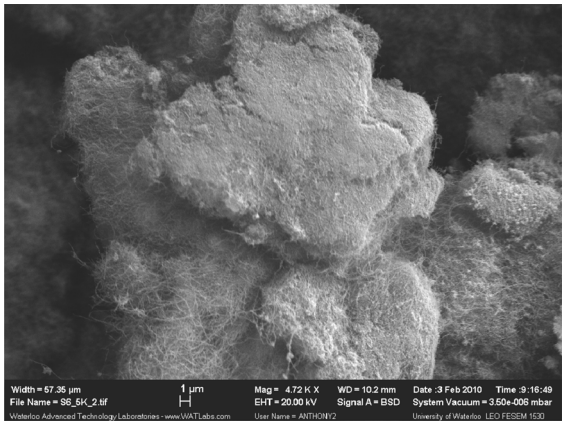

Figure 21. Spent $Ni_{0.5}Ca_{2.5}Al$ catalyst after 20 h of CO_2 reforming of CH_4 (5,000 × magnification).

4. Conclusion

Different approaches for the synthesis gas production using Ni-supported catalysts have been investigated. The typical methods to produce synthesis gas (partial oxidation and CO_2 reforming of CH_4) by HT-like catalyst were performed for short and long reaction periods in order to the investigate the effects of the structure of the catalyst on the stability and reactivity. Partial oxidation, CO_2 reforming and the oxidative CO_2 reforming of CH_4 processes to produce synthesis gas were evaluated at 700 ℃ for 20 h in the presence of three different catalysts: $Ni_{0.5}Mg_{2.5}Al$, $Ni_{0.5}Ca_{2.5}Al$, and Ni/Al_2O_3. For the partial oxidation of CH_4 during 20 h of reaction, the $Ni_{0.5}Mg_{2.5}Al$, $Ni_{0.5}Ca_{2.5}Al$, and Ni/Al_2O_3 catalysts exhibited similar levels of activity, which were close to the equilibrium levels, with the Ca- and Mg-containing samples exhibited no deactivation and the Ni/Al_2O_3 catalyst being deactivated. During CO_2 reforming of CH_4, the Ni/Al_2O_3 and $Ni_{0.5}Ca_{2.5}Al$ catalyst conversions decreased as a result of coke formation, leading to deactivation of the catalyst. The $Ni_{0.5}Mg_{2.5}Al$ catalyst exhibited high and stable reactivities for over 100 h. The Oxidative CO_2 reforming of CH_4, which combined the exothermic partial oxidation with the endothermic CO_2 reforming of CH_4, can facilitate heat transfer between the reactions. The addition of O_2 reduced coke deposition on the catalysts since the oxygen can combust the surface carbon. Therefore, the catalytic activity levels for the partial oxidation and the oxidative CO_2 reforming of CH_4 processes could be maintained close to the equilibrium levels with less deactivation compared to the CO_2 reforming of CH_4. The $Ni_{0.5}Ca_{2.5}Al$ catalyst exhibited the highest initial activity, but was deactivated quickly due to coke deposition. The $Ni_{0.5}Mg_{2.5}Al$ catalyst exhibited the most stable reactivity over 20 h of reaction. Additionally, the $Ni_{0.5}Mg_{2.5}Al$ catalyst exhibited excellent stability for the CO_2 reforming of CH_4, even in the absence of oxygen in the feed gas. TPR data indicate stronger interactions between the Ni and Mg compared to that with Ca, which seemingly correlates to catalyst stability in terms of decreased coke formation and subsequently allowing conversions and product yields to remain constant.

Acknowledgments

The authors gratefully acknowledge Technology Convergence Inc. (TCI) and the Ontario Centres of Excellence (OCE) for financial support, and a grant from Korea Institute of Energy Research (KIER) under Korea Research Council for Industrial Science and Technology, the Ministry of Knowledge and Economy, South Korea.

References

1. González, A. R., Asencios, Y. J. O., Assaf, E. M., and Assaf, J. M., "Dry Reforming of Methane on Ni-Mg-Al Nano-Spheroid Oxide Catalysts Prepared By the Sol-gel Method from Hydrotalcite-like Precursors," *Appl. Surf. Sci.*, **280,** 876-887 (2013).
2. Tang, S., Lin, J., and Tan, K. L., "Partial Oxidation of Methane to Syngas over Ni/MgO, Ni/CaO and Ni/CeO_2," *Catal. Lett.*, **51,** 169-175 (1998).
3. Di, M., Dajiang, M., Xuan, L., Maochu, G., and Yaoqiang, C., "Partial Oxidation of Methane to Syngas over Monolithic Ni/gama-$A1_2O_3$ Catalyst - Effects of Rare Earths And other Basic Promoters," *J. Rare Earths*, **24,** 451-455 (2006).
4. Choudhary, V. R., Rane, V. H., and Rajput, A. M., "Beneficial Effects of Cobalt Addition To Ni-catalysts for Oxidative Conversion of Methane to Syngas," *Appl. Catal. A Gen.*, **162,** 235-238 (1997).
5. Shinozuka, Y., Ohishi, Y., Shishido, T., Takaki, K., and Takehira, K., "Nickel Containing Mg-Al Hydrotalcite-type Anionic Clay Catalyst for the Oxidation of Alcohols with Molecular Oxygen," *J. Mol. Catal. A Chem.*, **236,** 206-215 (2005).
6. Bhattacharyya, A., Chang, V. W., and Schumacher, D. J., "CO_2 Reforming of Methane to Syngas I: Evaluation of Hydrotalcite Clay-derived Catalysts," *Appl. Clay Sci.*, **13,** 317-328 (1998).
7. Bartholomew, C. H., "Mechanisms of Catalyst Deactivation," *Appl. Catal. A Gen.*, **212,** 17-60 (2001).
8. Ito, M., Tagawa, T., and Goto, S., "Suppression of Carbonaceous Depositions on Nickel Catalyst for the Carbon Dioxide Reforming of Methane," *Appl. Catal. A Gen.*, **177,** 15-23 (1999).
9. Takehira, K., Shishido, T., Wang, P., Kosaka, T., and Takaki, K., "Autothermal Reforming of CH_4 over Supported Ni Catalysts Prepared from Mg-Al Hydrotalcite-like Anionic Clay," *J. Catal.*, **221,** 43-54 (2004).
10. Sukenobu, M., Morioka, H., Kondo, M., Wang, Y., Takaki, K., and Takehira, K., "Partial Oxidation of Methane over Ni/Mg-Al Oxide Catalysts Prepared by Solid Phase Crystalliza-

tion Method from Mg-Al Hydrotalcite-like Precursors," *Appl. Catal. A Gen.*, **223,** 35-42 (2002).

11. Tomishige, K., Nurunnabi, M., Maruyama, K., and Kunimori, K., "Effect of Oxygen Addition to Steam and Dry Reforming of Methane on Bed Temperature Profile over Pt and Ni Catalysts," *Fuel Process. Technol.*, **85,** 1103-1120 (2004).
12. Basini, L., Amore, M. D, Fornasari, G., Guarinoni, A., Matteuzzi, D., Del Piero, G., Trifirò, F., and Vaccari, A., "Ni/Mg/Al Anionic Clay Derived Catalysts for the Catalytic Partial Oxidation of Methane Residence Time Dependence of the Reactivity Features," *J. Catal.*, **173,** 247-256 (1998).
13. Inaba, M., Tsunoda, T., Suzuki, K., Takehira, K., and Hayakawa, T., "Combined Partial Oxidation and Dry Reforming of Methane to Synthesis Gas over Noble Metals Supported on Mg-Al Mixed Oxide," *Appl. Catal. A Gen.*, **275,** 149-155 (2004).
14. Sukenobu, M., Morioka, H., Furukawa, R., Shirahase, H., and Takehira, K., "CO_2 Reforming of CH_4 over Ni/Mg-Al Oxide Catalysts Prepared by Solid Phase Crystallization Method from Mg-Al Hydrotalcite-like Precursors," *Catal. Lett.*, **73,** 21-26 (2001).
15. Olsbye, U., Akporiaye, D., Rytter, E., Rønnekleiv, M., and Tangstad, E., "On the Stability of Mixed M^{2+}/M^{3+} Oxides," *Appl. Catal. A Gen.,* **224,** 39-49 (2002).
16. Shiraga, M., Atake, I., Shishido, T., Oumi, Y., Sano, T., and Takehira, K., "Partial Oxidation of Propane over Ru Promoted Ni/Mg(Al)O Catalysts: Self-activation and Prominent Effect of Reduction-oxidation Treatment of the Catalyst," *Appl. Catal. A Gen.*, **321,** 155-164 (2007).
17. Oyama, S. T., "Novel Catalysts for Advanced Hydroprocessing: Transition Metal Phosphides," *J. Catal.*, **216,** 343-352 (2003).
18. Bradford, M. C. J., and Vannice, M. A., "CO_2 Reforming of CH_4 over Supported Pt Catalysts," *J. Catal.*, **171,** 157-171 (1998).
19. Ruckenstein, E., and Wang, H. Y., "Combined Catalytic Partial Oxidation and CO_2 Reforming of Methane over Supported Cobalt Catalysts," *Catal. Lett.*, **73,** 99-105 (2001).
20. Amin, N. A. S., and Yaw, T. C., "Thermodynamic Equilibrium Analysis of Combined Carbon Dioxide Reforming with Partial Oxidation of Methane to Syngas," *Int. J. Hydro. Energy*, **32,** 1789-1798 (2007).
21. Zhu, Y.-A., Chen, D., Zhou, X.-G., and Yuan, W.-K., "DFT Studies of Dry Reforming of Methane on Ni Catalyst," *Catal. Today*, **148,** 260-267 (2009).
22. Zhang, Y., Xiong, G., Sheng, S., and Yang, W., "Deactivation Studies over NiO/γ-Al_2O_3 Catalysts for Partial Oxidation of Methane to Syngas," *Catal. Today*, **63,** 517-522 (2000).
23. Ginsburg, J. M., Pin, J., Solh, T. El, and Lasa, H. I. De., "Coke Formation over A Nickel Catalyst Under Methane Dry Reforming Conditions: Thermodynamic and Kinetic Models," *Ind. Eng. Chem. Res.*, **44,** 4846-4854 (2005).
24. Hu, Y. H., and Ruckenstein, E., "Temperature-programmed Desorption of CO Adsorbed on NiO/MgO," *J. Catal.*, **311,** 306-311 (1996).
25. Arena, F., Frusteri, F., Parmaliana, A., Plyasova, L., and Shmakov, N., "Effect of Calcination on the Structure of Ni/MgO Catalyst: an X-ray Diffraction Study," *J. Chem. Soc., Faraday Trans.*, **92,** 469-471 (1996).
26. Świerczyński, D., Libs, S., Courson, C., and Kiennemann, A., "Steam Reforming of Tar from a Biomass Gasification Process over Ni/olivine Catalyst Using Toluene as a Model Compound," *Appl. Catal. B Environ.*, **74,** 211-222 (2007).
27. Ruckenstein, E., and Hu, Y. H., "Carbon Dioxide Reforming of Methane over Nickel/Alkaline Earth Metal Oxide Catalysts," *Appl. Catal. A Gen.*, **133,** 149-161 (1995).
28. Shimizu, Y., Sukenobu, M., Ito, K., Tanabe, E., Shishido, T., and Takehira, K., "Partial Oxidation of Methane to Synthesis Gas over Supported Ni Catalysts Prepared from Ni-Ca/Al-layered Double Hydroxide," *Appl. Catal. A Gen.*, **215,** 11-19 (2001).